NANS-mediated synthesis of sialic acid is required for brain and skeletal development

van Karnebeek, Clara D M ; Bonafé, Luisa ; Wen, Xiao-Yan ; Tarailo-Graovac, Maja ; Balzano, Sara ; Royer-Bertrand, Beryl ; Ashikov, Angel ; Garavelli, Livia ; Mammi, Isabella ; Turolla, Licia ; Breen, Catherine ; Donnai, Dian ; Cormier, Valerie ; Heron, Delphine ; Nishimura, Gen ; Uchikawa, Shinichi ; Campos-Xavier, Belinda ; Rossi, Antonio ; Hennet, Thierry ; Brand-Arzamendi, Koroboshka ; Rozmus, Jacob ; Harshman, Keith ; Stevenson, Brian J ; Girardi, Enrico ; Superti-Furga, Giulio ; Dewan, Tammie ; Collingridge, Alissa ; Halparin, Jessie ; Ross, Colin J ; Van Allen, Margot I ; et al

Abstract: We identified biallelic mutations in NANS, the gene encoding the synthase for N-acetylneuraminic acid (NeuNAc; sialic acid), in nine individuals with infantile-onset severe developmental delay and skeletal dysplasia. Patient body fluids showed an elevation in N-acetyl-D-mannosamine levels, and patient-derived fibroblasts had reduced NANS activity and were unable to incorporate sialic acid precursors into sialylated glycoproteins. Knockdown of nansa in zebrafish embryos resulted in abnormal skeletal development, and exogenously added sialic acid partially rescued the skeletal phenotype. Thus, NANS-mediated synthesis of sialic acid is required for early brain development and skeletal growth. Normal sialylation of plasma proteins was observed in spite of NANS deficiency. Exploration of endogenous synthesis, nutritional absorption, and rescue pathways for sialic acid in different tissues and developmental phases is warranted to design therapeutic strategies to counteract NANS deficiency and to shed light on sialic acid metabolism and its implications for human nutrition.

DOI: https://doi.org/10.1038/ng.3578

NANS-mediated synthesis of sialic acid is required for brain and skeletal development

Clara D.M. van Karnebeek[1,2*], Luisa Bonafé[3*], Xiao-Yan Wen[4*], Maja Tarailo-Graovac[2,5], Sara Balzano[6], Beryl Royer-Bertrand[3,6], Angel Ashikov[7], Livia Garavelli[8], Isabella Mammi[9], Licia Turolla[10], Catherine Breen[11], Dian Donnai[11], Valerie Cormier[12], Delphine Heron[12], Gen Nishimura[13], Shinichi Uchikawa[14], Belinda Campos-Xavier[3], Antonio Rossi[15], Thierry Hennet[16], Koroboshka Brand-Arzamendi[4], Jacob Rozmus [1], Keith Harshman[17], Brian J. Stevenson[18], Enrico Girardi[19], Giulio Superti-Furga[19,20], Tammie Dewan [1], Alissa Collingridge [1], Jessie Halperin [1], Colin J. Ross [1,2,5], Margot I. Van Allen [2], Andrea Rossi[21], Udo F. Engelke[22], Leo A.J. Kluijtmans[22], Ed van der Heeft[22], Herma Renkema[22], Arjan de Brouwer[23], Karin Huijben[22], Fokje Zijlstra[22], Thorben Heisse[24], Thomas Boltje[24], Wyeth W. Wasserman[2,5], Carlo Rivolta[6], Sheila Unger[25], Dirk J. Lefeber [22,7], Ron A. Wevers[22 **], Andrea Superti-Furga[3, 26**]

these authors contributed equally to this work

***joint senior authors*

1 Department of Pediatrics, University of British Columbia, Vancouver, Canada

2 Centre for Molecular Medicine, Child & Family Research Institute, University of British Columbia, Vancouver, Canada

3 Centre for Molecular Diseases, Lausanne University Hospital (CHUV), University of Lausanne, 1011 Lausanne, Switzerland

4 Zebrafish Centre for Advanced Drug Discovery, Keenan Research Centre for Biomedical Science, St. Michael's Hospital; Dept. of Medicine, University of Toronto, Toronto, Ontario, Canada

5 Department of Medical Genetics, University of British Columbia, Vancouver, Canada

6 Department of Medical Genetics, University of Lausanne, Lausanne, Switzerland

7 Department of Neurology, Donders Institute for Brain, Cognition and Behavior, Radboud University Medical Center, Nijmegen, The Netherlands

8 Clinical Genetics Unit, IRCCS-S. Maria Nuova Hospital, Reggio Emilia, Italy

9 Ambulatorio di Genetica Medica ULSS 13, U.O. Ginecologia e Ostetricia, Ospedale Dolo, 30031 Dolo, Italy

10 Medical Genetics Unit, Local Health Authority (ULSS 9), Treviso, Italy

11 Manchester Centre for Genomic Medicine, Institute of Human Development, Faculty of Medical and Human Sciences, University of Manchester, St. Mary's Hospital, Central Manchester University Hospitals NHS Foundation Trust, Manchester Academic Health Science Centre, Manchester, UK

12 Institut IMAGINE, Necker-Enfants Malades Hospital, Paris, France;

13 Department of Radiology, Tokyo Metropolitan Children's Medical Center, Tokyo, Japan

14 Department of Orthopedics, National Center for Child Health and Development, Tokyo, Japan

15 Department of Molecular Medicine, Unit of Biochemistry, University of Pavia, 27100 Pavia, Italy

16 Department of Physiology, University of Zürich, 8057 Zürich, Switzerland

17 Genomic Technologies Facility, Faculty of Biology and Medicine, University of Lausanne, Lausanne, Switzerland

18 Vital-IT Group, Swiss Institute of Bioinformatics, University of Lausanne, Lausanne, Switzerland

19 CeMM Research Center for Molecular Medicine of the Austrian Academy of Sciences, 1090 Vienna, Austria

20 Center for Physiology and Pharmacology, Medical University of Vienna, Vienna Austria

21 Neuroradiology Department, G. Gaslini Children's Hospital, 16148 Genova, Italy

22 Translational Metabolic Laboratory, Department Laboratory Medicine, Radboud University Medical Centre, Nijmegen, The Netherlands

23 Department of Genetics, Radboud University Medical Centre, Nijmegen, The Netherlands

24 Department of Organic Chemistry, Radboud University, Nijmegen, The Netherlands

25 Medical Genetics Service, Lausanne University Hospital, University of Lausanne, 1011 Lausanne, Switzerland

26 Department of Pediatrics, Lausanne University Hospital, University of Lausanne, 1011 Lausanne, Switzerland

Address correspondence to ASF (asuperti@unil.ch), RW (ron.wevers@radboudumc.nl), or CvK (cvankarnebeek@cw.bc.ca)

Key words: NANS gene, N-acetyl neuraminic acid synthase, CDG, skeletal dysplasia, sialic acid biosynthesis, developmental delay, N-acetyl mannosamine, next generation metabolic screening

We identified bi-allelic mutations in *NANS*, the gene coding for *N*-acetyl-neuraminic acid (NeuNAc; sialic acid) synthase, in nine individuals with infantile-onset severe developmental delay and skeletal dysplasia. Patient body fluids showed an elevation of *N*-acetyl-mannosamine, and patient-derived fibroblasts had reduced NANS activity and were unable to incorporate sialic acid precursors into sialylated glycoproteins. Knockdown of *nansa* in zebrafish embryos resulted in abnormal skeletal development and exogenously added sialic acid partially rescued the skeletal phenotype. Thus, NANS-mediated synthesis of sialic acid is required for early brain development and skeletal growth. Normal sialylation of plasma proteins was observed in spite of NANS deficiency. Exploration of endogenous synthesis, nutritional absorption, and rescue pathways of sialic acid in different tissues and developmental phases is warranted to design therapeutic strategies for NANS deficiency and to shed light on sialic acid metabolism and its implications for human nutrition.

Intellectual developmental disorders (IDDs) affect 2-2.5% of children and adults worldwide[1]. The developmental origin is reflected in its definition as "substantial impairments of intellectual function and social or adaptive functioning present from early childhood"[2]. Recent advances

have shown that in many cases, the etiology is genetic, most frequently due to *de novo* mutations[3,4]. Along with better understanding of the surrounding condition and prognosis, insights into the molecular basis of neurocognitive impairment allows for the development and application of targeted therapeutic strategies[5]. Although less frequent than IDD, genetic disorders affecting skeletal development and growth (commonly called the "skeletal dysplasias") are a group of over 500 distinct disorders[6]. Studying their molecular basis has provided precious insights into the many factors necessary for skeletal development, ranging from minerals and structural molecules to enzymes, to signaling molecules and transcription factors[6,7]. We report here a genetic disorder presenting with a combination of severe IDD with skeletal dysplasia and short stature. Our data show that its pathogenic basis is an inborn error of metabolism that affects the endogenous synthesis of *N*-acetyl neuraminic acid (NeuNAc; sialic acid). Exploration of the biochemical and molecular features of this disorder provides new information on the role of sialic acid in the development of brain and bone.

RESULTS

Clinical and radiographic phenotype of NANS deficiency

The clinical patient reports are presented *in extenso* in the Supplementary Material. Nine patients from six families were studied; patients 1, 2, and 5 have been previously described[8,9]. The main clinical features are as follows: prenatal history was unremarkable in all patients except for one

(pt. 8), in whom prenatal hydrocephalus was diagnosed. No specific signs and symptoms were present at birth except for disproportionately short limbs that were observed in three patients (pts. 3, 8 and 9). In the first months of life, all patients showed muscle hypotonia, and the achievement of early developmental milestones such as sitting and walking was delayed. Subsequently, global developmental delay, including cognitive impairment, was the major medical concern. All adult patients showed moderate to severe IDD; only one patient acquired speech and none was living independently. Seizures were a prominent and early feature in one patient but were infrequent in some and absent in others. Social competences were relatively preserved. Body measurements at birth were normal or slightly reduced, but growth velocity decreased during the first or the second year of life, and short stature with shortening of both the trunk and the limbs was present in all adult patients. The facial features showed a prominent forehead, mild synophrys, a sunken nasal bridge, a prominent bulbous nasal tip, and full lips (Fig. 1). No endocrine anomalies were noticed and adult patients had gone through pubertal development. Neuro-imaging was available in six patients: patient 8 showed prenatal-onset hydrocephalus, while patient 9 showed perisylvian polymicrogyria, small basal ganglia and reduced white matter (Supplementary Figure 1); the other four patients showed moderate cerebral atrophy with nonspecific white matter changes. Distinct features that permitted to distinguish these individuals among the large group of persons with severe IDD were the facial dysmorphisms and the skeletal dysplasia with short stature, premature carpal ossification, platyspondyly, longitudinal metaphyseal striations, and small epiphyses (see Fig. 1 for details).

For more radiographic details, see also the previous clinical reports of patients 1 and 2[8] and patient 5[9] (pat. 1 in that reference).

Identification of *NANS* mutations and functional analysis

Exome sequencing was performed on genomic DNA from patients 1 to 4 (two couples of sibs). After the filtering pipeline (see Methods and Supplementary Table 1), only one gene, *NANS*, showed biallelic variants in all four patients (Table 1). A small insertion/deletion just 5' of exon 4, c.449-10_449-5delGATTACinsATGG, was seen at heterozygosity in all four patients (reference transcript: ENST00000210444, NCBI Reference Sequence: NM_018946.3). In addition to this shared mutation, patients 1 and 2 (who were sisters) had a single nucleotide insertion predicted to result in a frameshift with early truncation (c.389_390insT, p.Lys131Gln*fs*Ter8), while patients 3 and 4 (who were brother and sister) had a canonical splice donor site mutation (c.448+1G>A). Computational haplotype reconstruction using exome data revealed a specific haplotype encompassing a region of 1.38 MB on chromosome 9 (from 9:100388119 (rs10817858) to 9:101767385 (rs41305481)) in the four individuals carrying the intronic insertion/deletion, indicative of a common origin. Sanger sequencing was used to confirm the mutations and to verify segregation with disease in all families. To test for pathogenicity of these variants, *NANS* cDNA was retrotranscribed from fibroblasts or lymphoblastoid cell RNA from patients 1, 3, and 4, as well as the parents of patients 3 and 4, incubated with or without cycloheximide, PCR-amplified and analyzed by capillary electrophoresis (Supplementary figure 2). The c.449-10_449-

5delGATTACinsATGG insertion/deletion (patients 1, 2, 3 and 4) resulted in very low levels of mRNA, with presence of wild-type mRNA as well as an isoform lacking both exons 3 and 4 (in-frame); in presence of cycloheximide, this allele appeared to produce additional abnormally isoforms, that apparently were subject to NMD. The c.448+1G>A variant (patients 3 and 4) produced two splicing isoforms, one lacking both exons 3 and 4 (similar to the previous mutation) and expressed at levels comparable to the wild-type allele, and very low levels of an out-of-frame isoform lacking exon 3 and part of exon 4. The exonic insertion c.389_390insT (patients 1 and 2) triggered nonsense-mediated RNA decay (NMD), as shown by sequencing of RT-PCR clones obtained from cells with or without cycloheximide. Thus, all three mutations resulted either in unstable or nonfunctional *NANS* mRNA or in reduced levels of wild-type transcripts. We then screened patients 5, 6, 7, and 8 by selective PCR amplification of *NANS* exons from genomic DNA and direct bi-directional Sanger sequencing of the amplicons, and found bi-allelic mutations in all patients, including four missense mutations and one triplet insertion leading to the duplication of one amino acid (Table 1 and Fig. 2).

Investigation of patient 9, the youngest patient in our series, followed a different course; he was enrolled into the TIDEX study which combines genomics and metabolomics screening[10]. Metabolomic screening had revealed an unusual metabolite, *N*-acetylated mannosamine (ManNAc), in plasma and urine of this child (see below). Among the variants identified by exome sequencing in this patient, two missense mutations in *NANS* stood out as ManNAc-

phosphate is the substrate of the NANS enzyme and malfunction of this enzyme would have accounted for the ManNAc accumulation in body fluids. The *NANS* variants identified in patient 9 were confirmed via Sanger sequencing and shown to segregate correctly in the family. Of note, the exome results of patients 1, 2, 3, 4 and 5 were examined for possible pathogenic mutations in the *GNE* gene (see below) and none was observed. After this stage, the data of patients 1-8 and those of patient 9 were combined for all subsequent studies.

Mapping of mutations on the 3D protein model of NANS

The NANS protein was modeled as a homo-dimer based on the *Neisseria* homolog, as well as on recent results supporting dimer formation for the human protein[11]. Of the predicted amino acid changes (Table 1), four mapped in or near the active site: p.Lys131Gln, p.Gly133Val, p.Tyr188His, and p.Pro189Leu. It is likely that any of these would affect the catalytic activity of the enzyme, either by changing the ability of the protein to bind substrate (p.Lys131 and p.Tyr188 are also predicted to make H-bonds with the substrates[11], fig 2), by changing the pocket shape (p.Gly133Val) or by affecting functional residues in the active site (p.Pro189 is located right next to p.Tyr188). Mutations p.His29Asn and p.Arg237Cys are localized at the dimer interface and likely affect the folding, protein stability and/or dimer formation. While close to the dimer interface, the p.Ile327 that is duplicated is not involved in protein contacts in our model and it could be affecting folding instead. Finally, p.Arg151His is located on the surface of

the protein and away from the dimer interface and substrate-binding site, possibly interfering with folding or with a critical protein interaction.

NANS mutations lead to accumulation of ManNAc *in vivo*

Next generation metabolic screening (see Methods) was first applied to cerebro-spinal fluid (CSF) of patient 9 (Figure 3 and Supplementary Table 2), and then to plasma of patients 1-4 and 9 (data not shown), leading to the identification of an unusual compound, *N*-acetyl mannosamine, in all 5 patients. Quantitative NMR spectroscopy was then used to determine the concentration of *N*-acetyl mannosamine in available patients' urine samples. In patients 1, 2, 3, 4 and 8 (all adults at the time of study), the urinary concentration of ManNAc ranged from 41 to 98 µmol/mmol creatinine (reference values, <10), whereas in patient 9 (age 3 years) excretion was highest (295 µmol/mmol creatinine). NMR spectroscopy was applied to homogenates of cultured fibroblasts to explore the intracellular sialic acid synthesis pathway. In fibroblasts from two unrelated patients (patients 3 and 9), this showed increased intracellular levels of *N*-acetylmannosamine-6-phosphate rather than of free ManNAc. NANS can act as a *N*-acetylneuraminic acid phosphate synthase (MIM 605202; EC 2.5.1.57). This may account for the accumulation of *N*-acetylmannosamine in body fluids and *N*-acetylmannosamine-6-phosphate within the cell. The free NeuNAc concentration in fibroblasts was normal (supplementary table ST2). Finally, we evaluated whether the deficient activity of NANS would lead to systemic deficiency of sialic acid. The concentration of free NeuNAc was evaluated in urine of 5 patients from 4 families (relative

to creatinine excretion) as well as in the CSF of patient 9. In all patients, normal values were found (Supplementary Table 3) suggesting that there was no systemic depletion of free neuraminic acid. Analysis of plasma transferrin- and apolipoprotein C-III isoforms, to evaluate the biosynthesis of N- and O-glycans respectively, has been done repeatedly on several of the patients in the clinical setting as well and given normal results (Supplementary Table 4), further contributing to the notion that peripheral sialylation was not significantly affected despite NANS deficiency.

NANS mutations impair enzyme activity

In two preliminary experiments, we explored the sialylation of proteins and lipids at the cell surface of patient and control fibroblasts using FITC-labelled *Sambucus nigra* lectin (that specifically binds to terminal galactose-bound sialic acid residues) and FACS analysis, and we determined the cellular content of CMP-NeuNAc and total NeuNAc before and after addition of 10 mM ManNAc[12] . No differences between patient and control fibroblasts were seen, possibly because the concentration of ManNAc used was significantly higher than what is found physiologically. We then developed a method to measure NANS enzyme activity in cell lysates by incubation with ManNAc-6-P and phosphoenolpyruvate (PEP) and quantification of newly formed NeuNAc by mass spectrometry (Fig. 3, panel D). In comparison with five healthy controls (613+/-150 nmol NeuNAc/mg protein, mean +/-SD), the three available patient fibroblast lines showed reduced production of NeuNAc (163+/-111 nmol NeuNAc/mg protein,

mean +/-SD) at 24h incubation. Fibroblasts from the heterozygous father of patient 3 and 4 showed intermediate NANS activity (403 nmol NeuNAc/mg protein). Although the residual activity in this assay was high, these results were in agreement with an autosomal recessive defect in NANS.

Incorporation of ManNAc into sialoglycoproteins is impaired

We then used metabolic labeling of sialic acids using propargyloxycarbonyl(Poc)-derivatized analogs of ManNAc and NeuNAc (ManNPoc and NeuNPoc, respectively) [13], a recently developed technique that had been useful to confirm deficient sialic acid incorporation in cells deficient for the Golgi transporter of CMP-sialic acid[14]. NeuNPoc, which enters the metabolic pathway downstream of the enzymatic step catalyzed by NANS, was incorporated efficiently into glycoproteins in all cell lines analyzed, while ManNPoc, which enters the pathway upstream (Fig. 4), was incorporated in fibroblasts from a control and from a NANS heterozygote, but not in those of patients 3, 8, and 9 (Fig. 3). These data confirmed the functional impairment of NANS activity on the metabolic pathway of sialic acid biosynthesis and protein sialylation. NANS deficiency should therefore be included among the list of CDGs (congenital disorders of glycosylation). Importantly, these data suggest that exogenous NeuNAc might be used to bypass the enzymatic block (see Discussion, below).

nansa knockdown perturbs zebrafish skeletal development

There are two zebrafish orthologs for the human *NANS* gene, the *nansa* and *nansb* genes (see Methods for detail). *Nansa* is expressed during early embryonic development including stages of 50% epiboly in the axis, 1-13 somites at the notochord and polster, and 14-19 somites at the hatching gland. Thereafter, *nansa* is strongly expressed in the head, immature eye, myotome, optic tectum and pharyngeal arch skeleton [15]. The expression pattern of *nansb* is unknown. We designed splicing morpholinos to knockdown both *nansa* and *nansb* genes [16] (see Methods). Microinjection of *nansa* morpholino into the newly fertilized zebrafish eggs resulted in embryos with small head, pericardial edema, and developmental anomalies of the skeleton, revealed by alcian blue staining, at 6dpf (Fig. 5 A, B). Interestingly, *nansa* morphants showed a complex phenotype in the area of the head, including hypoplastic or absent of Meckel's cartilage, lack of basihyal, shortened and abnormal ethmoid plate, trabecula, parachordal, palatoquadrate, and absence of the ceratobranchial structures (Fig. 5 B) [17]. *Nansb* knockdown morphants did not show an overt phenotype even at higher concentrations of morpholinos (data not shown).

Partial rescue of skeletal development by exogenous NeuNAc

Given the position of *nansa* (and NANS) in the synthetic pathway of NeuNAc (see above), we tested whether the addition of sialic acid in zebrafish embryo water would rescue the head and skeleton developmental phenotypes of *nansa* zebrafish morphants. Sialic acid at 200 μM resulted in partial rescue of the skeletal phenotype as measured by the reappearance and development of Meckel's cartilage structure; this was correctly formed in 9% of embryos in basic *nansa*

knockdown conditions, but in 61% of embryos when sialic acid was added to the water (Fig. 5 C, D). Interestingly, the rescue effect of sialic acid was time-dependent; rescue was observed when sialic acid was added to the fish water right after morpholino injection, but not when it was added 24 hours post fertilization, suggesting that sialic acid plays a critical role in early embryonic development, potentially in cartilage and skeleton cell lineage specification or growth.

DISCUSSION

We present evidence that biallelic deleterious mutations in *NANS* are associated with a severe intellectual developmental disorder and skeletal dysplasia. First, we identified 10 different *NANS* variants in 9 patients from 6 unrelated families, segregating according to a recessive disease model. Second, the *NANS* mutations impaired the activity of the *N*-acetyl-neuraminic acid synthase enzyme as evidenced by reduced enzyme activity and by the specific block of *N*-acetyl mannosamine analogue incorporation in cultured cells. Third, dysfunction of NANS *in vivo* was confirmed by the accumulation of substrates of the missing enzyme: *N*-acetyl mannosamine in body fluids, and *N*-acetyl-mannosamine 6-phosphate in cultured cells. Finally, inactivation of the enzyme activity in zebrafish embryos resulted in a complex phenotype including abnormal development of skeletal structures. The conclusion that *NANS* mutations are the cause of the clinical phenotype is strengthened by the fact it was reached by two independent approaches. Patients 1 to 8 were ascertained because of their phenotype of intellectual disability and specific

skeletal dysplasia, and the genomic approach led to identification of *NANS* mutations and to their validation through RNA studies. Patient 9 was subjected to metabolomic screening first in order to elucidate the cause of severe IDD and dysmorphisms, leading to the identification of ManNAc in body fluids, and this biochemical phenotype allowed to prioritize the *NANS* mutations as the most likely pathogenic amongst the variants found subsequently on exome sequencing. Although most of our patients were ascertained retrospectively and the clinical assessment is heterogeneous, there are indications for different degrees of clinical severity. The study of additional patients is needed to determine the clinical spectrum of NANS deficiency and to establish possible genotype-phenotype correlations.

Brain contains the highest concentration of total sialic acid among human organs[18]. Sialic acid is present on glycoproteins and glycolipids such as the gangliosides, that are particularly abundant in nervous tissue, and NANS is highly expressed in the human brain (Supplementary Figure 3). Genetic deficiency of either sialyltransferase ST3GAL3 (MIM#604402) or ST3GAL5 (MIM#609056), two enzymes that utilize CMP-NeuNAc to add terminal sialic acid residues to the glycosidic antennae of glycoproteins and glycolipids, leads to infantile epilepsy and/or developmental arrest, suggesting that appropriately sialylated glycoproteins and/or glycolipids are necessary for higher brain functions[19-22]. Mutations in the CMP-NeuNAc transporter SLC35A1 (MIM#605634; see Fig. 4) result in developmental disability with ataxia and bleeding diathesis [23]. The observation of IDD in NANS-deficient patients and the brain dysplasia observed

in two of them underlines the relationship between sialylation and neurologic functions and indicates that the requirements for sialic acid in the developing brain must be met at least partially by endogenous synthesis of sialic acid through the NANS pathway.

The short stature and skeletal dysplasia in NANS-deficient individuals also tells us that NANS-mediated sialic synthesis plays a pivotal role in skeletal development, specifically at the growth plate cartilage. The skeletal anomalies seen in the zebrafish knockdown model confirmed this notion. The avascular nature of cartilage may make it dependent on endogenous synthesis. Several of the key players in cartilage and bone growth and development, such as chondroitin sulfate proteoglycans[24], bone sialoprotein[25] and osteopontin[26], are heavily sialylated and will be candidates for further studies.

Tests detecting hyposialylated transferrin and apolipoprotein C-III yielded normal results in our NANS-deficient patients, and there was no clinical or laboratory evidence of hyposialylation of plasma proteins or clotting factors, suggesting that sialylation of plasma proteins is not significantly affected. How is sialylation achieved with impaired NANS activity? Several lines of explanation can be considered. First, the mutations in our patients may allow for some residual activity; none of our patients had a combination of two *bona fide* null alleles. Secondly, endogenous NeuNAc synthesis may be rate limiting in certain tissues and at certain times, where and when synthetic requirements are maximal (such as in the brain, in periods of rapid growth

before birth and in the first two years of life[27-29], or in cartilage during infancy and childhood), but not in other tissues where synthetic requirements for sialic acid may be lower. Such a mechanism has been put forward to explain the muscle-restricted phenotype of GNE myopathy (MIM# 603824)[30], a disorder caused by recessive mutations in the *GNE* gene coding for UDP-*N*-acetylglucosamine 2-epimerase and ManNAc kinase activities in the sialic acid synthesis pathway (Fig. 4). Thirdly, some tissues may be able to rescue and recycle sialic acid derived from the lysosomal breakdown of sialylated macromolecules (see Fig. 4). A fourth possibility, not mutually exclusive with the others, is that nutrition-derived sialic acids may be entered into biosynthetic pathways, and that this may occur in some tissues, such as the liver, but not, or to a lesser extent, in brain or cartilage. The observation of normal levels of free sialic acid in the urine of our NANS-deficient patients also indicates that there is no systemic depletion of sialic acid.

The role of nutrition-derived sialic acid raises the question of a possible treatment with oral sialic acid in NANS-deficient individuals, in analogy to other glycosylation and sialylation defects, such as CDG1B (MIM# 602579) and GNE myopathy[31], that have been amenable to treatment by oral administration of specific sugars. Some of our data may indeed point in this direction. When added to patients' cells in culture, the sialic acid analogue NeuNPoc (used because of its detectability), but not the upstream metabolite ManNPoc, was able to bypass the enzymatic block and be incorporated into macromolecules. In zebrafish embryos, exogenously added sialic acid was able to partially recue the developmental phenotype caused by *NANS* knockdown. Could

345 dietary supplementation with sialic acid be beneficial for NANS deficient patients? There is
346 evidence that free sialic acid can be taken up and metabolized by cultured cells[32]; this could occur
347 through pinocytosis and release to the cytoplasm by the lysosomal sialic acid exporter (SLC17A5;
348 Fig. 4). In animal models, sialic acid injected in the peritoneum is incorporated into
349 macromolecules[33], and orally administered free sialic acid is found in plasma and subsequently in
350 the liver and the brain[29,33]. N-glycolyl-neuraminic acid, a sialic acid analogue that is widespread in
351 mammals and apes but absent in man because of an evolutionary mutation, is found in human
352 tissues as the result of dietary uptake from meat products[34,35]. Altogether, there is evidence
353 indicating that alimentary sialic acids can be taken up and incorporated into biosynthetic
354 pathways in the human. The relative contributions of endogenously synthesized, nutritionally
355 derived, and rescued sialic acid in different tissues and at different developmental stages in man
356 remain to be investigated and may explain how the consequences of NANS deficiency are
357 restricted to the developing brain and cartilage. Particularly, if the brain pathology in NANS
358 deficiency occurs in the first months of life (and perhaps even prenatally), this might be an
359 obstacle to efficient treatment. Extensive studies in cell culture and *in vivo* are needed before
360 envisaging any treatment possibility for NANS-deficient individuals. Such studies would also
361 have the potential of clarifying the role of nutritional sialic acid in the human (see below).
362
363 Human milk contains a high concentration of free oligosaccharides, most of which are
364 sialylated[27,28,36,37], as well as free sialic acid. These oligosaccharides, that are notably absent from

365 cow's milk and infant formulas, have been attributed numerous functions, including stimulating
366 brain development and cognition in infants[27,28,37,38]. Since oral administration of sialic acid in
367 humans is considered safe and well-tolerated, nutritional supplementation with sialic acid in
368 infancy, gestation and advanced age has been proposed[27-29,37]. In view of the role and potential of
369 sialic acid in nutrition, exploring the pathogenesis of brain dysfunction and skeletal dysplasia
370 induced by NANS deficiency is worthwhile not only to elaborate therapeutic approaches for
371 NANS-deficient individuals, but also to shed light on sialic acid metabolism with its implications
372 for human nutrition.

373

374 **URLs**

375

376 The Exome Aggregation Consortium database: http://exac.broadinstitute.org/ (accessed January
377 2016)
378 The Wellderly database at Scripps Wellderly Genome Resource, The Scripps Wellderly Study, La
379 Jolla, CA: stsi-ftp.sdsc.edu (accessed January 2016)
380 The PhiloP software for mutation assessment: http://genetics.bwh.harvard.edu/pph2/
381 The Provean software for mutation assessment: http://provean.jcvi.org/index.php
382 The Zebrafish genes database (for accession numbers ENSDART0000006708 and
383 ENSDART00000169540), www.zfin.org

The Novoalign software, www.novocraft.com

The Gaslini Cell Repository and Biobank, dppm.gaslini.org/biobank/

The Leenaards Foundation in Lausanne, www.leenaards.ch

The Treatable Intellectual Disability Endeavour in British Columbia: 1st Collaborative Area of Innovation, www.tidebc.org

The Rare Diseases Models and Mechanisms Network, www.rare-diseases-catalyst-network.ca/index.php

Acknowledgements. This work has been supported by funding from the Leenaards Foundation in Lausanne; the Faculty of Biology and Medicine of the University of Lausanne; the B.C. Children's Hospital Foundation (Treatable Intellectual Disability Endeavour in British Columbia: 1st Collaborative Area of Innovation); Genome BC (SOF-195 grant); the Rare Diseases Foundation; the Rare Diseases Models and Mechanisms Network; the Canadian Institutes of Health Research (#301221 grant); the Dutch Organisation for Scientific Research, ZONMW (Medium Investment Grant 40-00506-98-9001 and VIDI Grant 91713359 to DJL). The zebrafish studies were supported by funding to XYW from Canadian Rare Disease Models and Mechanisms Network, Brain Canada Foundation, Natural Sciences and Engineering Research

Council of Canada (NSERC) and Canada Foundation for Innovation (CFI). The informatics infrastructures were supported by Genome BC and Genome Canada (ABC4DE Project) as well as by the Vital-IT Project of the SIB-Swiss Institute of Bioinformatics (Lausanne). CJDR is funded by CIHR New Investigator Award. CvK is a recipient of the Michael Smith Foundation for Health Research Scholar Award (Vancouver, CA). EG is supported by Marie Skłodowska-Curie fellowship (MSCA-IF-661491). We thank Dr. M. Filocamo at the Gaslini Biobank (Genova, Italy) for a fibroblast line of Patient 1. We thank Alexandre Reymond (CIG, FBM, Université de Lausanne) and his lab for lymphocyte immortalization. We thank Carole Chiesa for Sanger sequencing and sample handling and shipment; Siebolt de Boer for excellent technical assistance; B. Toh at UBC for metabolic sample handling; X. Han for Sanger sequencing; Bryan Sayson for consenting and data management; M. Higginson for DNA extraction and sample handling; A. Ghani for administrative assistance. We also thank Roderick Houben for skillfully preparing figure 4, and Andi Bandi for all other figures. We are grateful to our clinical colleagues in Dolo, Genova, Lausanne, Manchester, Paris, Reggio Emilia, Tokyo, Treviso, and Vancouver for patient management. ASF dedicates this paper to the memory of Professor Paolo Durand who pointed out the relationship between sialic acid metabolism and IDD to him in 1980. Finally, we wish to thank the patients reported here as well as their parents for the enthusiasm they showed towards our research efforts, their patience challenged by the studies lasting many years, and for their repeated donation of biologic samples. They have been the source of continuous motivation for us.

Author Contributions - CVK, LB, SU, RW and ASF conceived the study, coordinated and supervised the different teams. ASF, LB, CVK, TW, AC, MVA, JH, LG, LT, LC, VC, DH, DD, CB, IM, and ShUc and recruited the patients, reviewed the clinical and radiographic features and obtained biologic materials from patients. ASF, SU, and GN reviewed the radiographic data. JR performed the bone marrow studies. Andrea Rossi reviewed the cerebral imagings. KH, BS, BCX, SB, BRB, HR, CR, MT, WW, and AdB were responsible for exome sequencing, haplotype reconstruction, Sanger sequencing, database studies, and mRNA/cDNA studies. RW, LK, EvdH, UE performed the metabolomics studies. Antonio Rossi studied ManNAc incorporation on fibroblasts. THennet performed the lectin binding studies. AA, KH, FZ and DL performed the NANS enzyme assay. DL, AA, THeisse, TB studied the incorporation of sialic acid precursors in lymphocytes and fibroblasts. EG and GSF obtained the 3D model and mapped the affected amino acid residues. XYW, KB-A generated and phenotyped the zebrafish model. CVK and ASF prepared the manuscript with contributions from all coauthors. All coauthors edited and reviewed the final manuscript.

Competing financial interests statement: The authors declare no competing financial interests.

REFERENCES

1. Salvador-Carulla, L. *et al.* Intellectual developmental disorders: towards a new name, definition and framework for "mental retardation/intellectual disability" in ICD-11. *World Psychiatry*. **10**, 175–180 (2011).

2. American Psychiatric Association. Diagnostic and statistical manual of mental disorders (5th Ed). (Washington, D.C., 2013).

3. de Ligt, J. *et al.* Diagnostic exome sequencing in persons with severe intellectual disability. *New Engl. J. Med.* **367,** 1921-9 (2012).

4. Gilissen, C. *et al.* Genome sequencing identifies major causes of severe intellectual disability. *Nature* 511, 344-7 (2014).

5. Van Karnebeek, C.D.M. & Stockler, S. Treatable inborn errors of metabolism causing intellectual disability: a systematic literature review. *Mol. Genet. Metab*. **105**, 368–381 (2012).

6. Bonafé, L. *et al.* Nosology and classification of genetic skeletal disorders: 2015 revision. *Am. J. Med. Genet*. **167**:2869-92 (2015)

466 7. Superti-Furga, A., Bonafé, L., Rimoin, D.L. Molecular-pathogenetic classification of genetic
467 disorders of the skeleton. *Am. J. Med. Genet.* **106**:282-93 (2001)
468
469 8. Camera, G., Camera, A., Di Rocco, M., Gatti, R. Sponastrime dysplasia: report on two siblings
470 with metal retardation. *Pediatr. Radiol.* **23**, 611-4 (1993).
471
472 9. Geneviève, D. *et al.* Exclusion of the dymeclin and PAPSS2 genes in a novel form of
473 spondyloepimetaphyseal dysplasia and mental retardation. *Eur. J. Hum. Genet.* **13**:541-6 (2005).
474
475 10. Tarailo-Graovac, M. *et al.* Exome sequencing and the management of neurometabolic
476 disorders. *New Engl. J. Med.* **in the press** (2016)
477
478 11. Cotton, T.R., Joseph, D.D., Jiao, W. & Parker, E.J. Probing the determinants of
479 phosphorylated sugar-substrate binding for human sialic acid synthase. *Biochim. Biophys. Acta.*
480 **1844**, 2257-2264 (2014).
481
482 12. Galuska, S.P. *et al.* Quantification of nucleotide-activated sialic acids by a combination of
483 reduction and fluorescent labeling. *Anal. Chem.* **82**, 4591-4598 (2010).
484

13. Büll, C. *et al*. Sialic acid glycoengineering using an unnatural sialic acid for the detection of sialoglycan biosynthesis defects and on-cell synthesis of siglec ligands. *ACS Chem. Biol.* **10**, 2353-2363 (2015).

14. Riemersma, M. et al. Disease mutations in CMP-sialic acid transporter SLC35A1 result in abnormal α-dystroglycan O-mannosylation, independent from sialic acid. *Hum. Mol. Genet*. **24,** 2241-6 (2015)

15. Link V, Shevchenko A, Heisenberg CP. Proteomics of early zebrafish embryos. *BMC Dev. Biol*. **6**, 1 (2006)

16. Eisen JS, Smith JC. Controlling morpholino experiments: don't stop making antisense. *Development* **135,** 1735-43 (2008)

17. Javidan, Y., Schilling, T.F. Development of cartilage and bone. *Methods Cell Biol.* **76,** 415-36. (2004)

18. Wang, B. & Brand-Miller, J. The role and potential of sialic acid in human nutrition. *Eur. J. Clin. Nutr*. **57**, 1351–69 (2003).

505 19. Simpson, M. A. *et al.* Infantile-onset symptomatic epilepsy syndrome caused by a
506 homozygous loss-of-function mutation of GM3 synthase. *Nature Genet*. **36**, 1225-1229 (2004).
507
508 20. Hu, H. *et al.* ST3GAL3 mutations impair the development of higher cognitive functions. *Am.*
509 *J. Hum. Genet*. **89**, 407-414 (2011).
510
511 21. Fragaki, K. *et al.* Refractory epilepsy and mitochondrial dysfunction due to GM3 synthase
512 deficiency. *Eur. J. Hum. Genet*. **21**, 528-534 (2013).
513
514 22. Boccuto, L., *et al.* A mutation in a ganglioside biosynthetic enzyme, ST3GAL5, results in salt
515 & pepper syndrome, a neurocutaneous disorder with altered glycolipid and glycoprotein
516 glycosylation. *Hum. Mol. Genet*. **23,** 418-433 (2014).
517
518 23. Mohamed M et al. Intellectual disability and bleeding diathesis due to deficient CMP--sialic
519 acid transport. *Neurology* **81**:681-7 (2013)
520
521 24. Roughley, P.J., White, R.J., Santer, V. Comparison of proteoglycans extracted from high and
522 low weight-bearing human articular cartilage, with particular reference to sialic acid content. *J.*
523 *Biol. Chem.* **256**:12699-704 (1981).
524

525 25. Vincent, K., Durrant, M.C. A structural and functional model for human bone sialoprotein. *J.*
526 *Mol. Graph. Model.* **39**:108-17 (2013).
527
528 26. Sodek, J., Ganss, B., McKee, M.D. Osteopontin. *Crit. Rev. Oral Biol. Med.* **11**:279-303 (2000).
529
530 27. Wang, B. Sialic acid is an essential nutrient for brain development and cognition. *Annu. Rev.*
531 *Nutr.* **29**, 177-222 (2009).
532
533 28. Wang, B. Molecular mechanism underlying sialic acid as an essential nutrient for brain
534 development and cognition. *Adv. Nutr.* **3**, 465S-472S (2012).
535
536 29. Sprenger, N. & Duncan, P.I. Sialic acid utilization. *Adv. Nutr.* **3**, 392S-397S (2012).
537
538 30. Salama, I. *et al.* No overall hyposialylation in hereditary inclusion body myopathy myoblasts
539 carrying the homozygous M712T GNE mutation. *Biochem. Biophys. Res. Commun.* **328**, 221-226
540 (2005).
541
542 31. Malicdan, M.C.1, Noguchi, S., Hayashi, Y.K., Nonaka, I. & Nishino, I. Prophylactic treatment
543 with sialic acid metabolites precludes the development of the myopathic phenotype in the
544 DMRV-hIBM mouse model. *Na.t Med.* **15**, 690-695 (2009).

32. Oetke, C. *et al*.. Evidence for efficient uptake and incorporation of sialic acid by eukaryotic cells. *FEBS Eur. J. Biochem*. **268**, 4553-4561 (2001).

33. Nöhle, U., & Schauer, R. Uptake, metabolism and excretion of orally and intravenously administered, 14C- and 3H-labeled *N*-acetylneuraminic acid mixture in the mouse and rat. *Hoppe Seylers Z. Physiol. Chem*. **362**, 1495-506 (1981).

34. Tangvoranuntakul, P. *et al.* Human uptake and incorporation of an immunogenic nonhuman dietary sialic acid. *Proc. Natl. Acad. Sci. USA*, **100**, 12045-12050 (2003).

35. Samraj, A. N. *et al.* A red meat-derived glycan promotes inflammation and cancer progression. *Proc. Natl. Acad. Sci. USA*, **112**, 542-547 (2015).

36. Bode, L. Human milk oligosaccharides: every baby needs a sugar mama. *Glycobiology* **22**, 1147-1162 (2012).

37. Fuhrer, A. *et al.* Milk sialyllactose influences colitis in mice through selective intestinal bacterial colonization. *J. Exp. Med*. **207**, 2843–2854 (2010).

38. Röhrig, C.H., Choi, S.S. & Baldwin N. The Nutritional Role of Free Sialic Acid, a Human Milk Monosaccharide, and Its Application as a Functional Food Ingredient. *Crit Rev Food Sci Nutr. Jun 26:0. [Epub ahead of print]* (2015).

571 **LEGENDS TO FIGURES**

572

573

574 Fig. 1. **Morphologic and skeletal features in NANS deficiency.**

575 A, B: patient 9 at age 6 months (A) and at age 3 years (B); C,D: patient 8 at age 28 years; E,F:
576 patient 4 at age 24 years; G,H; patient 3 at age 28 years; I,J: patient 2 at age 38 years; K,L: patient 1
577 at age 40 years. Only short limbs are apparent at age 6 months; facial dysmorphism with
578 prominent forehead, saddle nose, full lips and coarsening of traits is apparent at age 3 years. All
579 adult patients have short stature (height between 130 and 150 cm). All photographs obtained and
580 published with consent. M, N, O: lateral spine films show coronal clefts at birth (M, patient 8),
581 severe vertebral body dysplasia at age 3 (N, patient 9); in adulthood, the vertebral bodies have a
582 normal shape (O, patient 2). At the knees, there are metaphyseal striations and small epiphyses
583 (epi-metaphyseal dysplasia) at age 9 years (P, patient 8); in adulthood, epiphyses remain small
584 but metaphyseal striations have disappeared (Q, patient 2). Advanced carpal ossification at age
585 21 months (R, patient 9), and metaphyseal striations (distal radius) with epiphyseal dysplasia at
586 age 9 years (S, patient 8). Short femoral necks and small, irregular capital femoral epiphyses (epi-
587 metaphyseal dysplasia) at age 3 years 7 months (T, patient 9); in the adult (U, patient 3) short
588 femoral neck and small epiphyses but bone and cartilage structure appear normal. Compare the
589 radiographic images of patients 1 and 2 and patient 5 as reported earlier[8,9].

590

Fig. 2. 3D model of NANS protein and mapping of amino acid residues affected by mutations

A : Model of the human NANS protein, showing one monomer in grey and one in blue. Mutated residues are color-coded based on the patient with each allele mapped on a separate monomer. Lys131 and Arg151 are shown on both monomers. B and C: Detailed view of the location of the mutations. PEP: phosphoenolpyruvate.

Fig. 3. Evidence of impaired NANS activity *ex vivo* and in cell culture. A,B,C: 500 MHz 1D ^{1}H-NMR spectra of body fluids and model compounds: **A.** CSF of patient 9 containing *N*-acetylmannosamine at 180 µmol/L (reference <5). Resonances of alpha and beta forms of *N*-acetylmannosamine are shown in the inserts **B.** relevant part of the CSF spectrum (a), compared with the spectrum of ManNAc (b), GalNAc (c), and GlcNAc (d); **C.** Spectra obtained from fibroblasts of a control (a), patient 8 (b) and model compound ManNAc-6-P. **D**: NANS enzyme activity in fibroblast lysates. **E:** Metabolic labeling of sialylated proteins. Fibroblasts from a control (ctr), the heterozygous father of patients 3 and 4 (father), and patients 4, 8 and 9 (see table 1) were incubated with peracetylated propargyloxycarbonyl analogs of ManNAc and NeuNAc - ManNPoc and NeuNPoc respectively (see Fig. 4 for their entry point in the sialic acid biosynthetic pathway). Cell proteins were detected by Western blotting using streptavidin-HRP (upper panels) or antibodies against GAPDH (lower panels) as internal control. In cells from the control and from the heterozygous father, both ManNPoc and NeuNPoc result in strong labeling of proteins. In patients' cells, ManNPoc (that enters the synthetic pathways upstream of NANS)

611 is unable to label the proteins, while NeuNPoc (that enters downstream the NANS enzyme) is
612 incorporated efficiently. This confirms a metabolic block between ManNAc and NeuNAc,
613 consistent with impaired NANS activity.
614
615 **Fig. 4. Simplified scheme of *N*-acetyl neuraminic acid metabolism in the human.** Biosynthesis
616 of NeuNAc is achieved largely in the cytoplasm, except for the CMAS (**) reaction that takes
617 place in the nucleus (nuclear membrane and its possible transporters omitted here for
618 simplicity). The synthesis of *N*-acetyl mannosamine is carried out in two steps by the
619 bifunctional enzyme, GNE/ManNAc synthase (*). *N*-Acetyl-neuraminic acid synthase (NANS) is
620 indicated in red. CMP-sialic acid is transferred by a specific transporter, SLC35A1, into the
621 medial- and trans-Golgi where it is used as a substrate for the sialylation of proteins and lipids by
622 various sialyltransferases. - When sialylated glycoproteins and lipids are degraded in the
623 lysosome, the free sialic acid released by sialidases can diffuse out of the lysosome through the
624 lysosomal sialic acid transporter (SLC17A5). Free NeuNAc (as well as the non-human sialic acid,
625 NeuNGc) can be taken up by pinocytosis and released into the cytoplasm by the SLC17A5
626 transporter. Free sialic acid can then re-enter the biosynthesis pathway (indicated as “salvage” in
627 the scheme). The relative importance of biosynthesis and salvage in different cell types and
628 tissues is largely unknown. The metabolic scheme also shows the entry points of the two
629 synthetic analogs used in this study, ManPoc and NeuNPoc (see text), the first being upstream,
630 the second downstream of the step catalyzed by NANS.

Fig. 5. Abnormal skeletal development in *nansa* morpholino knockdown zebrafish is partially rescued by exogenous sialic acid. A, B: *nansa*-e3i3 morphants (4ng/nl) demonstrate small head, pericardial edema and abnormal cartilage and skeleton development including hypoplastic or absent of Meckel's cartilage (m) and lack of basihyal (bh), shortened and abnormal ethmoid plate (ep), trabecula (tr), parachordal (pch), palatoquadrate (pq) and ceratobranchial (cb) structures in dorsal and ventral view. Abbreviations used: lateral: m, Meckel's cartilage; bh, basihyal; dorsal: ep, ethmoid plate; tr, trabecula; pch, parachordal; ventral: m, Meckel's cartilage; ch, ceratohyal cartilage; cb, ceratobranchial; pq, palatoquadrate. **C, D**: 200 μM sialic acid partially rescued the abnormal skeletal phenotype as measured by Meckel's cartilage analysis. P1 - complete Meckel's cartilage. P2 - incomplete Meckel's cartilage, P3 - absent of Meckel's cartilage. The graph in D shows the proportion of fish showing a Meckel's cartilage phenotype of P1, P2 or P3 with or without exogenously added sialic acid. For each experimental condition, approx. 10-12 embryos were analyzed (actual numbers shown in the figure); experiments were done in triplicate. Bars represents SD between the triplicates. In the *nansa*–e313 morpholino treated animals, the difference between with or without 200 μM sialic acid is statistically significant: (*) p=0.05 for P1 embryos, and (**) p.=0.01 for P3 embryos (two-tailed T-test).

Table 1. Overview of NANS mutations observed in the nine patients.

genomic DNA position (chr. 9)	cDNA position*	exon	protein	presence in databases**	*PolyPhen****	*Provean *****	observed in patient(s)
100819175	c.85C>A	1	p.His29Asn	no	probably damaging	deleterious	Pat. 8
100839236	c.389_390insT	3	p.Lys131Gln*fs*Ter8	Wellderly: 0.0008	*n.a.*	*n.a.*	Pat. 1 and 2
100839249	c.398G>T	3	p.Gly133Val	no	probably damaging	deleterious	Pat. 6 and 7
100839300	c.448+1G>A	3	aberrant splicing of exons 3 and 4 as seen in mRNA studies	ExAC=0.00002633	n.a.	n.a.	Pat. 3 and 4
100840462	c.449-10_449-5delGATTACinsATGG§	4	aberrant splicing of exons 3 and 4 as seen in mRNA studies	ExAC = 0.00004947	n.a.	n.a.	Pat. 1 and 2 Pat. 3 and 4
100840478	c.452G>A	4	p.Arg151His	Wellderly: 0.0008	probably damaging	neutral	Pat. 5 (homozygous)
100840588	c.562T>C	4	p.Tyr188His	no	probably damaging	deleterious	Pat. 9
100840592	c.566C>T	4	p.Pro189Leu	no	probably damaging	deleterious	Pat. 8
100843203	c.709C>T		p.Arg237Cys	no	probably damaging	deleterious	Pat. 9
100845238	c.981insATC	6	p.Ile327dup	no	probably damaging	deleterious	Pat. 6 and 7

*Transcript: ENST00000210444 (CCDS6733) NCBI Reference Sequence: NM_018946.3; ** ExAC database: http://exac.broadinstitute.org/, accessed November 2015; Wellderly database: Scripps Wellderly Genome Resource, The Scripps Wellderly Study, La Jolla, CA (URL: stsi-ftp.sdsc.edu), accessed January 2016. – *** http://genetics.bwh.harvard.edu/pph2/- **** http://provean.jcvi.org/index.php

METHODS

Ethics - The studies were approved by the ethics boards of the following institutions: BC Children's & Women's Hospital, University of British Columbia (#12-00067), the Ethics Board of the Lausanne University Hospital. Research was performed according to the countries' ethics code of conduct. Parents or guardians provided written informed consent for the biochemical and genetic analysis and the publication of photographs and clinical data.

Identification of mutations in *NANS* – For patients 1 to 4, fragmented genomic DNA was purified with AMPure XP beads and its quality was assessed with an Agilent Bioanalyzer. Preparation of the exome enriched, barcoded sequencing libraries was performed using the SureSelect Human All Exon v4 kit (Agilent). The final libraries were quantified with a Qubit Fluorometer (Life Technologies) and the correct size distribution was validated on the Agilent Bioanalyzer. Libraries were then sequenced on a HiSeq 2000 machine (Illumina), generating 100 bp paired-end reads. Raw reads were aligned onto the hg19 reference genome using the Novoalign software. Data cleanup and variant calling were performed according to GATK Best Practices recommendations[39]. Variant filtering was made with Annovar[40] and with in-house *perl* and *bash* scripts, available upon request. For patient 9, who was genotyped in the Vancouver lab, similar procedures were used. To verify for the presence of a possible ancestral haplotype

carrying the *NANS* ins/del in patients 1 to 4, we extracted all SNP alleles that were present in the region surrounding NANS and that were listed in the dbSNP database. Local genotypes were then scored, and likely haplotypes were constructed. – In patients 5 to 8, all individual exons of *NANS* were amplified from genomic DNA (primers available upon request) and sequenced directly in both directions using the Sanger method. For patient 9, exome sequencing was performed as part of the TIDEX gene discovery project using using the Agilent SureSelect kit (Agilent Technologies) and Illumina HiSeq 2000 (Illumina). The sequencing reads were aligned to the human reference genome version hg19 (coverage 35X) and rare variants were identified and assessed for their potential to disrupt protein function. In total, we identified 19 candidate genes affected by 2 rare heterozygous variants. Of these, *NANS* stood out as the most interesting functional candidate because of the pre-existing next-generation metabolomics data. Sanger sequencing in the patient and his parents confirmed the mutations and segregation with disease.

Construction of a 3D protein model for NANS and mapping of the predicted mutations - A molecular model for the dimeric full-length human NANS protein was generated with I-TASSER[41], using as templates the *Neisseria meningitidis* homolog[42] and the human AFPL domain[43] structures. The model illustrations were generated with the PyMOL Molecular Graphics System, Version 1.7.4, Schrödinger, LLC.

mRNA studies - Lymphoblastoid cell lines were cultured in suspension under 5% CO2 in T25 flasks with RPMI Medium 1640 + GlutaMAX-I (Gibco) containing 10% FBS (Gibco, ref. 10270-106), 1% penicillin/streptomycin (Gibco), whereas fibroblasts were cultured in DMEM (1X) with 1g/L D-glucose L-glutamine (Gibco), supplemented with 10% FBS and 1% penicillin/streptomycin. To test for nonsense-mediated mRNA decay (NMD), treatment with cycloheximide (Sigma-Aldrich) was performed in parallel with controls by incubating 10 million cells for 4 hours in the presence of medium supplemented with 28 µg/ml of this chemical, according to published protocols[44]. Total RNA was isolated from both cycloheximide-treated and untreated fibroblast and lymphoblast cultures by using the Direct-zol RNA MiniPrep kit (Zymo Research) according to the manufacturer's instructions. cDNA was prepared following the retrotranscription of 500 ng RNA, by using the PrimerScript RT-PCR kit (Clontech) and random hexamers; 10 ng of the produced cDNA were then used as template for downstream experiments. A specific primer pair spanning the exon-exon junctions 1-2 and 5-6 (for sequences, see Supplementary Table 5) was designed to amplify the regions of the NANS cDNA containing all mutations studied. RT-PCRs were performed in triplicate in a final reaction volume of 20 µl containing 5X Green GoTaq reaction buffer (Promega), 100 µM dNTP mix, 200 nM of each primer, and 0.1 U of GoTaq G2 DNA Polymerase (Promega). Reactions were incubated at 94°C for 1 minute followed by 35 cycles at 93°C for 20 seconds, at 64.1°C for 30 seconds and 72°C for 1 minute. The obtained products were resolved by capillary electrophoresis with the eGene HDA-GT12 Multi-Channel Genetic Analyzer (eGene Inc.), quantified, and finally ligated into the

709 pCRII-TOPO TA vector (Invitrogen). Ligation mixes were used to transform chemically
710 competent TOP-10 E. coli cells (Invitrogen), and individual clones (at least 30 clones per
711 electrophoresed sample) were sequenced by direct Sanger sequencing using BigDye terminator
712 V1.1 (Applied Biosystems) with insert-specific primers. Sequencing data were analyzed using the
713 CLC Bio software (Qiagen) and compared with the corresponding human reference sequence
714 (build hg19).
715
716 **Next generation metabolomics analysis** - High resolution untargeted metabolomics analysis of
717 body fluids was performed using UHPLC-Qtof mass spectrometry. Cerebrospinal fluid and
718 heparinised plasma samples were deproteinised in methanol/ethanol (50:50 v/v; 100 µL sample
719 plus 400 µL methanol/ethanol). Samples were analysed in duplicate. Two µL sample was applied
720 to an Acquity HSS T3 reversed phase column (100 x 2.1 mm; 100Å, 1.8 µm) and an Agilent 6540
721 UHD accurate mass UHPLC Qtof-MS with acquisition in positive and negative mode was used.
722 Buffers in positive mode consisted of A: 0.1v/v% formic acid/water, B: 0.1 vv% formic acid in
723 water/methanol (1:99 v/v) was used while in negative mode A: 10 mM acetic acid, B: 10 mM
724 acetic acid in water/ methanol (1:99 vv). After analysis and XCMS alignment, in house developed
725 bioinformatics software showed the features (exact m/z, retention time and intensity) deriving
726 from metabolites that are significantly different in intensity in the patient sample compared to
727 age- and sex-matched controls. The Human Metabolome Database 3.0 was used to putatively
728 annotate significantly different features[45] This technique, also referred to as "next generation

metabolic screening", was clinically validated using body fluids of patients with 25 known inborn errors of metabolism and introduced in the Nijmegen patient care research setting.

Proton NMR spectroscopy of body fluids, fibroblast homogenates and model compounds of *N*-acetylated sugars was performed on a 500 MHz NMR spectrometer with minor modifications[46]. The NMR spectrum of fibroblasts was recorded on a homogenate obtained after sonification of 7.5 10^6 cells in D_2O. The homogenate was deproteinised over a 10 kD filter and trimethylsilyl-2,2,3,3-tetradeuteropropionic acid (=TSP) was used as a chemical shift reagent in the NMR spectrum. The model compounds *N*-acetylmannosamine, *N*-acetylgalactosamine, *N*-acetylglucosamine were purchased from Sigma chemicals and *N*-acetylmannosamine-6-phosphate from Carbosynth (disodium salt).

Lectin staining on cultured fibroblasts - Fibroblasts were cultured for 48 h in DMEM 10%FCS supplemented with 0, 1, and 10 mM ManNAc. After incubation, fibroblasts were trypsinized, washed twice in Hanks buffered saline solution (HBSS) containing 1% FCS and resuspended at 1 x 10^6 cells/ml. Aliquots of 10^5 cells (100 ul) were incubated with 1mM FITC-labeled Sambucus nigra lectin (Vector Labs) in HBSS for 20 min on ice, washed twice in HBSS containing 1% FCS, and analyzed by flow cytometry using a FACScanto II cytometer (BD Biosciences).

748 **ManNAc incorporation in fibroblast culture** - Skin fibroblasts were cultured and expanded in
749 DMEM containing 10% FCS at 37 °C in 5% CO_2, and then for 24 hours in the absence of FCS.
750 For the incorporation experiment, mycoplasma-negative cells were incubated in DMEM, without
751 serum and antibiotics, with or without 10 mM *N*-acetylmannosamine (ManNAc), at 37°C in 5%
752 CO_2 for 48 h. After incubation, the medium was removed, cells were harvested in PBS and
753 collected by low speed centrifugation. The cell pellet was sonicated in 20 mM Tris-HCl, pH 8.0, 5
754 mM EDTA, 150 mM NaCl, 1 μg aprotinin and 1 mM PMSF and the lysate ultracentrifuged at
755 30.000 × g for 1 h at 4 °C to pellet the membrane fraction. In the clear supernatant, protein
756 content was determined with the BCA protein assay (Pierce) and aliquots of the supernatant
757 were ultrafiltered with Amicon Ultra-0.5 Centrifugal Filter Unit with a cut-off of 3kDa to
758 separate sialic acid from soluble protein. The dried filtrate was used for sialic acid analysis. The
759 CMP-sialic acid content was discriminated from free sialic acid by reduction: labelling with the
760 fluorophore 1,2-diamino-4,5-methylene-dioxybenzene (DMB) requires free keto as well as
761 carboxyl groups of the sialic acid molecule, and reduction of the keto group prior to the labelling
762 process precludes the labelling of non-activated sialic acid[12]. Each lyophilized sample was split in
763 two aliquots. To reduce free non activated monosaccharides dried samples were dissolved in 0.2
764 M sodium borate buffer, pH 8.0, containing 0.2 M sodium borohydride, incubated at 0°C o/n
765 and dried in a SpeedVac concentrator. For fluorescent labelling of sialic acid, samples were
766 hydrolyzed in 0.2 N trifluoroacetic acid (TFA) for 4 h at 80 °C, dried, redissolved twice in
767 methanol and dried again. To label sialic acids with DMB, hydrolysates were dissolved in 80 μl of

0.64 mg/ml DMB in 500 mM 2-mercaptoethanol, 9 mM sodium hydrosulfite, 20 mM TFA and incubated for 2 h at 56 °C. Reactions were then stopped by adding 10 µl of 0.2 M NaOH. The derivatized sialic acids were then quantified by HPLC on a binary pump system (1525µ Binary HPLC Pump, Waters) coupled to a fluorescence detector (2475 Multy λ Fluorescence Detector, Waters) set at λex 372 nm and λem 456 nm. Chromatography was carried out at room temperature with a LichroCART 250-4 Superspher 100 RP18 (250 × 4 mm) column (Merck) and LiChrospher 100 RP18 (25 × 4 mm) (Merck) as pre-column. Mobile phases were methanol/acetonitrile/water/TFA (4:4:92:0.1) and methanol/acetonitrile/water/TFA (45:45:10:0.1) and the flow rate was 0.3 ml/min[12].

Measurement of the NeuNAc content in fibroblasts – Fibroblasts (~2.5 millon cells) in 250 µl 50 mM Tris/HCl (pH 7.5) were sonicated on ice (3x 8 sec), then centrifuged (10 min, 10.000 g, 4 °C). To 100 µl of the supernatant (lysate) was added ^{13}C3-*N*-acetyl-neuraminic acid (± 23 µM) as internal standard and the solution was applied to a 30 kDa filter cup (Amicon Ultra) with 10 µl 2% formic acid in the collection tube for deproteination. After centrifugation for 30 min at 13.000 g and 4 °C, the flow-through was used for quantification of NeuNAc by mass spectrometry according to published methods[47,48]. Assays were performed in duplicate and NeuNAc levels were normalized for protein level in the lysates.

Determination on NANS activity in fibroblast cultures – Skin fibroblasts were obtained from affected individuals and healthy controls and cultured at 37.0°C under 5.0% CO_2 in culture medium E199, supplemented with 10% fetal calf serum and 1% Penicillin/Streptomycin. All cultures were tested for mycoplasma infection prior to cultivation. We developed an assay for NANS activity as follows: fibroblasts (~7.5 million cells) in 300 µl 50 mM Tris/HCl pH (7.5) were sonicated on ice (3x 8 sec), then centrifuged (10 min, 10.000 g, 4 °C). The supernatant (lysate) was used for protein determination (BCA assay) and for enzyme activity assay. Incubation of *N*-acetyl-D-mannosamine-6-phosphate disodium salt (Carbosynth, 2 mM) and 20 µl lysate was done at 37 °C in duplicate in a total reaction volume of 100 µl. The reaction buffer consisted of 50 mM Tris/HCl (pH 7.5), 3 mM phosphoenol-pyruvate (PEP; Roche), and 1 mM $MgCl_2$. Control incubations without ManNAc-6-P were subtracted as a blanc from the incubations. The reactions were allowed to proceed for 2.5, 5, and 24 hours and then stopped by freezing (-20 °C). Samples (100 µl) were deproteinized by addition of 50 µl ^{13}C3-*N*-acetyl-neuraminic acid (± 23 µM) as internal standard, centrifugation for 30 min at 13.000 g and 4 °C on a 30 kDa filter cup (Amicon Ultra), and the flow-through was collected in 10 µl 2% formic acid. NeuNAc levels were quantified by mass spectrometry as described[47,48] and normalized for protein level in the lysates.

Metabolic labeling of sialic acids and glycoproteins in fibroblast cultures

Skin derived fibroblasts were cultured in M199 medium (PAN biotech) supplied with 10% fetal bovine serum (PAA), non essential amino acids (NEAA) (Gibco), 100 U/mL

Penicilline/streptomycine (Gibco) and tested for mycoplasma contamination. Eighty percent confluent cells were further grown for 5 days in medium containing 15 μM of Ac5NeuNAc, Ac4ManNPoc, or Ac5NeuNPoc. Cells were collected in PBS by scraping and lysed in 150 mM NaCl, 50 mM TRIS-HCl, pH 7.5, 5 mM EDTA, 0.1% SDS, 1% Triton X-100, and 1× cOmplete® protease inhibitor cocktail (Roche). To biotinylate propargyloxycarbonyl-containing glycoproteins, cell lysates were resolved on 10% SDS gels, blotted on polyvinylidene fluoride (PVDF) membrane and after blocking of unoccupied membrane sites with 5% dry milk in PBS, incubated with 500 μM $CuSO_4$, 250 μM l-histidine, 100 μM azide-PEG3-biotin, 500 μM sodium ascorbate in PBS for 1h at 37°C. Biotinylated sialoglycoproteins were visualized by incubation with Horseradish Peroxidase conjugated Streptavidin (GE Healthcare), followed by signal development with SuperSignal™ West Femto Maximum Sensitivity Substrate (Thermofisher Scientific). As a loading control an immunostaining with Anti-GAPDH (Abcam Cat N ab8245) of the same western blots was used. Based on this protocol, we found that NeuNPoc at 15 μM concentration would readily label cellular sialoglycans after 5 days of incubation. For ManNPoc at the same concentration of 15 μM, longer incubation times were required to obtain strong labeling of glycoconjugates in fibroblasts from healthy donors (Figure 5).

Determination of glycosylation of plasma proteins - Analysis of plasma transferrin N-glycosylation was done by isoelectric focusing[49] as well as by nanochip QTOF mass

826 spectrometry50. The mucin-type O-glycosylation of plasma apolipoprotein CIII was done by
827 isoelectric focusing[49].
828
829 **Zebrafish studies** - Zebrafish were maintained at 28.5 C in a 10/14-h dark/light cycle. Protocols
830 for experimental procedures were approved by the Research Ethics Board of St. Michaels
831 Hospital, Toronto, Canada (protocol number ACC660). To knock down gene expression, we
832 used splicing blocking morpholino oligonucleotides (MO) for *nansa* and *nansb* knockdown plus
833 a standard control MO (ctrl MO) (for sequences, see Supplementary Table 5). The zebrafish
834 *nansa* gene has six exons with the translation start codon in exon 1 (access number
835 ENSDART0000006708; chr. 1). we designed a splicing blocking morpholino *nansa-e3i3* that can
836 block the splicing donor of exon 3, resulting in intron 3 retention and a truncated protein in
837 translation (data not shown). *Nansb* also has 6 exons with translation start codon in exon 1
838 (access number ENSDART00000169540; chr. 25) and we designed a morpholino *nansb-e1i1* to
839 block the splicing donor site of exon 1 of *nansb*, resulting in intron 1 retention and a truncated
840 *nansb* protein (data not shown). MOs were synthesized by Gene Tools, LLC (for sequences, see
841 supplementary material) and microinjected individually or in combination into 1 cell stage
842 zebrafish embryos. We injected individually *nansa*-e3i3 (4ng/nl) and *nansb*-e1i1 (4 ng/nl) MOs,
843 and co-injected *nansa*-e3i3 (4 ng/nl)/*nansb*-e1i1 (4 ng/nl) MOs. Each injection was repeated at
844 least three times. Knock-down of *nansa* and *nansb* was confirmed by RT-PCR to confirm
845 splicing defect and retention of the intron (data not shown). For control MO, embryos were

injected at 1 cell stage with 4 ng/nl. At least 30 embryos were injected per condition and included in the analysis. At 24 hpf, embryos were manually dechorionated. Total RNA was extracted from embryos at 48 hpf using TRIzol (Invitrogen). The RNA concentration of each sample was quantified using a NanoDrop ND-1000 spectrophotometer (NanoDrop Technologies). RNA integrity was verified in 1% agarose gel electrophoresis. The RNA template was converted into cDNA using Superscript II reverse transcriptase (Invitrogen), and used to amplify a *nansa* specific cDNA (for primer sequences, see Supplementary Table 5).

To visualize the cartilaginous structures, Alcian blue (Sigma) was dissolved in 70% ethanol and 1% hydrochloric acid. The zebrafish embryos (6 dpf) were fixed in 4% paraformaldehyde overnight at 4 C, and maintained in 100% methanol at -20 ^{0}C until processing. The embryos were washed with phosphate-buffered saline with 0.1% Tween-20 (PBST). The embryos were bleached in 30% hydrogen peroxide for 2 hours, washed with PBST and transferred into Alcian blue solution. Embryos were stained overnight at room temperature. The embryos were rinsed 4 times with acidified ethanol (HCl–EtOH) 5% hydrochloric acid, and 70% ethanol. Embryos were rinsed for 20 min in HCL-EtOH, and re-hydrated by washing 10 min in a HCL-EtOH/ H2Od series (75%, 25%, 50%, 50%, 25%, 75%) and 100% H2Od. Embryos were stored in 1 ml of glycerol-KOH.

866 **REFERENCES**

867

868 39. Van der Auwera, G.A. *et al.* From fastq Data to high-confidence variant calls: The genome
869 analysis toolkit test practices pipeline. *Curr. Protoc. Bioinformatics* **11**, 1-11 (2013).

870

871 40. Wang, K., Li, M. & Hakonarson H. ANNOVAR: Functional annotation of genetic variants
872 from next-generation sequencing data. *Nucleic Acids Res* **38**, e164 (2010).

873

874 41. Yang, J. *et al.* The I-TASSER Suite: protein structure and function prediction. *Nat. Methods* **1**,
875 7-8 (2015).

876

877 42. Gunawan, J. *et al.* Structural and mechanistic analysis of sialic acid synthase NeuB from
878 Neisseria meningitidis in complex with Mn2+, phosphoenolpyruvate, and *N*-
879 acetylmannosaminitol. *J. Biol. Chem.* **280**, 3555-3563 (2005).

880

881 43. Hamada, T. *et al.* Solution structure of the antifreeze-like domain of human sialic acid
882 synthase. *Protein Sci.* **15**, 1010-1016 (2006).

883

884 44. Rajavel, K.S. & Neufeld, E.F. Nonsense mediated decay of human HEXA mRNA. *Mol. Cell.*
885 *Biol.* **21**, 5512–5519 (2001).

45. Wishart DS, et al. HMDB 3.0 – The Human Metabolome Database in 2013. *Nucleic Acids Res.* **41**, D801- D807 (2013).

46. Engelke, U.F. *et al.* NMR spectroscopic studies on the late onset form of 3-methylglutaconic aciduria type I and other defects in leucine metabolism. *NMR Biomed.* **19**, 271-278 (2006).

47. Valianpour, F. *et al.* Quantification of free sialic acid in urine by HPLC-electrospray tandem mass spectrometry: a tool for the diagnosis of sialic acid storage disease. *Clin. Chem.* **50**, 403-9 (2004).

48. van der Ham, M. *et al.* Liquid chromatography-tandem mass spectrometry assay for the quantification of free and total sialic acid in human cerebrospinal fluid.
J. Chromatogr. B Analyt. Technol. Biomed. Life Sci. **878,** 1098-102 (2010)

49. Jansen, J.C. *et al.* CCDC115 Deficiency Causes a Disorder of Golgi Homeostasis with Abnormal Protein Glycosylation. *Am. J. Hum. Genet.* **98**, 310-21 (2016)

50. van Scherpenzeel, M. *et al.* High-resolution mass spectrometry glycoprofiling of intact transferrin for diagnosis and subtype identification in the congenital disorders of glycosylation. Transl Res. **166**, 639-649.e1 (2015)


A
C
E
G
I
K
B
D
F
H
J
L
M
N
O
P
Q
R
S
T
U

A

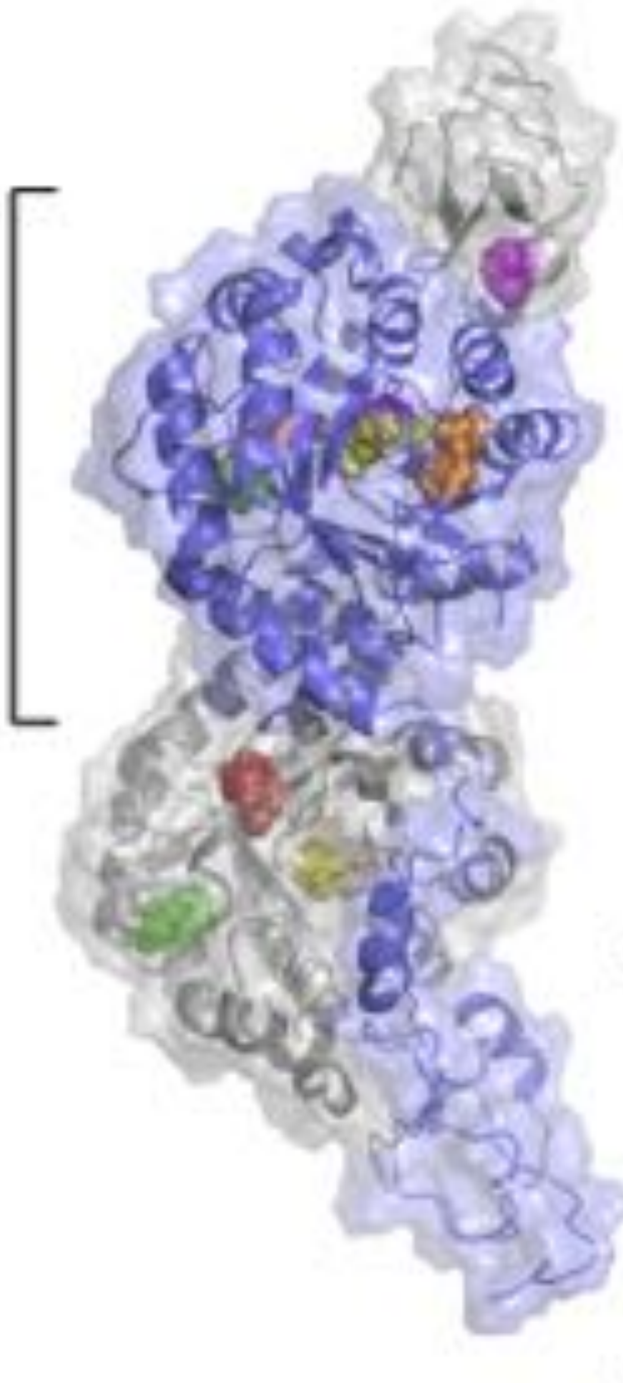
TIM barrel domain
AFPL domain

B

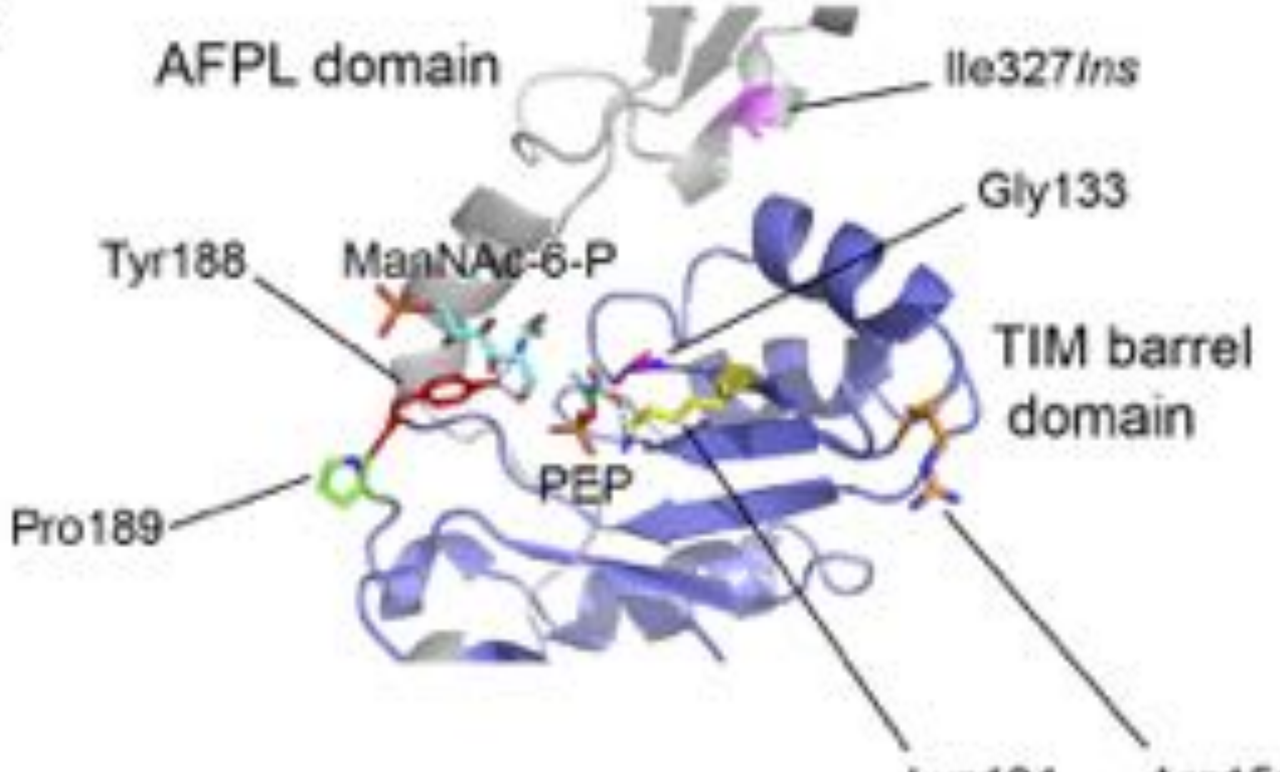
AFPL domain
Ile327Ins
Gly133
Tyr188
ManNAc-6-P
TIM barrel domain
PEP
Pro189
Lys131
Arg151

C

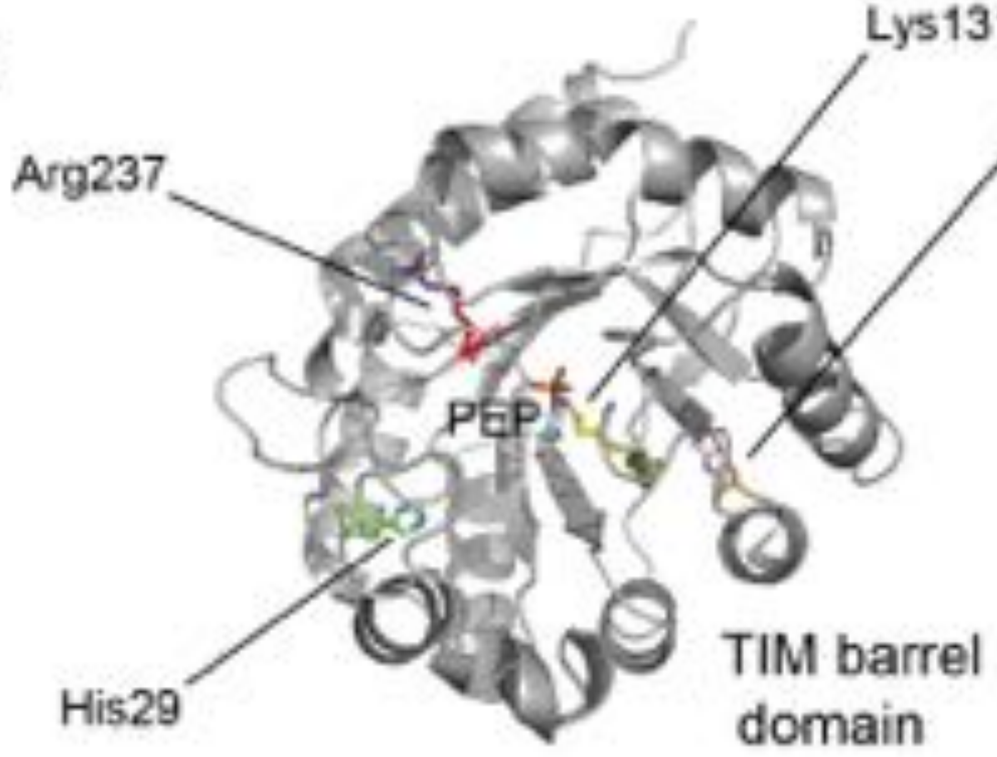
Arg237
PEP
His29
TIM barrel domain

A

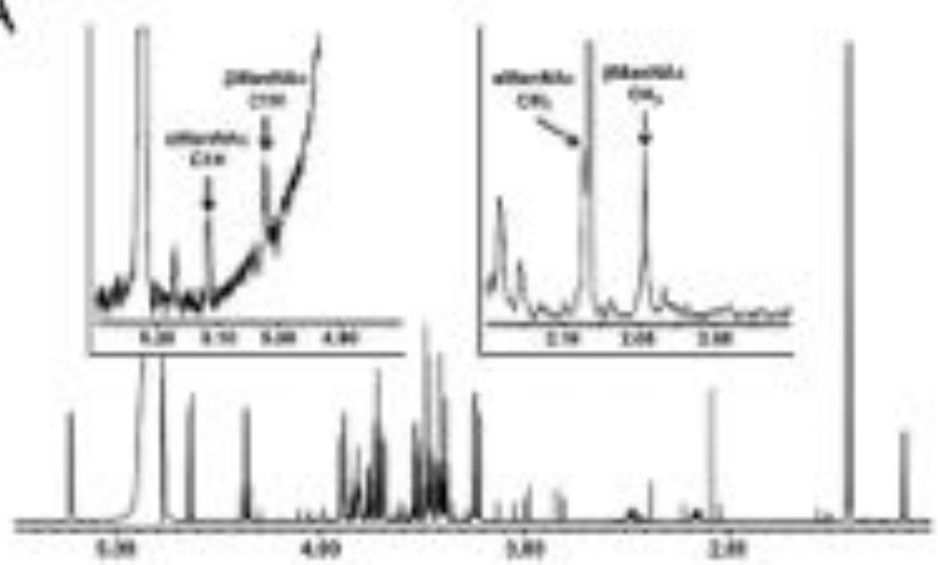

B

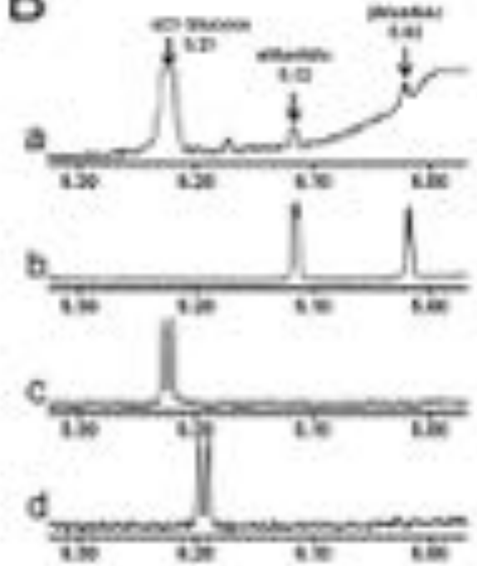
a
b
c
d

C

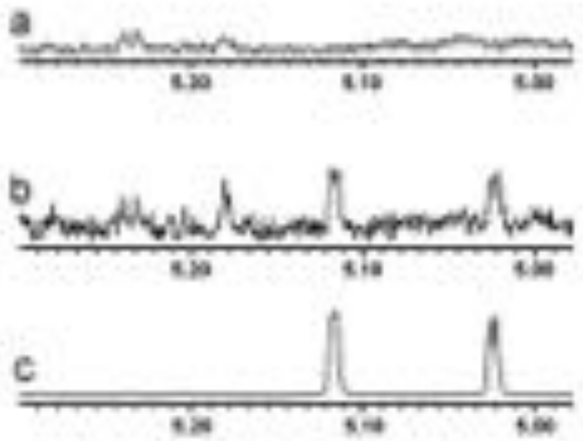
a
b
c

D

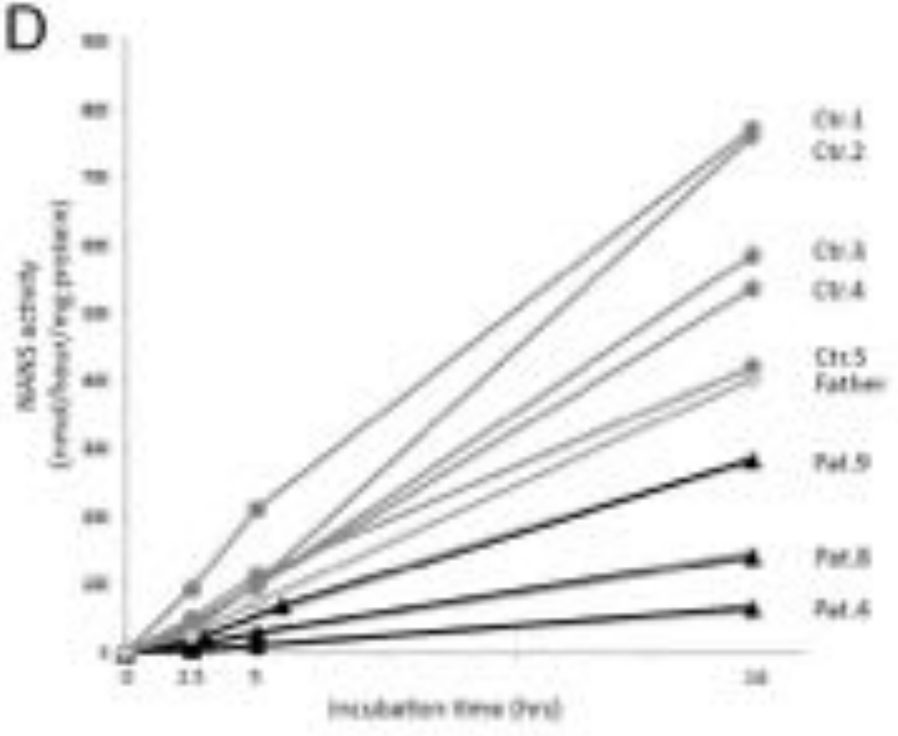
Ctr.1
Ctr.2
Ctr.3
Ctr.4
Ctr.5
Father
Pat.9
Pat.8
Pat.4
0
2.5
5
24
Incubation time (hrs)

E

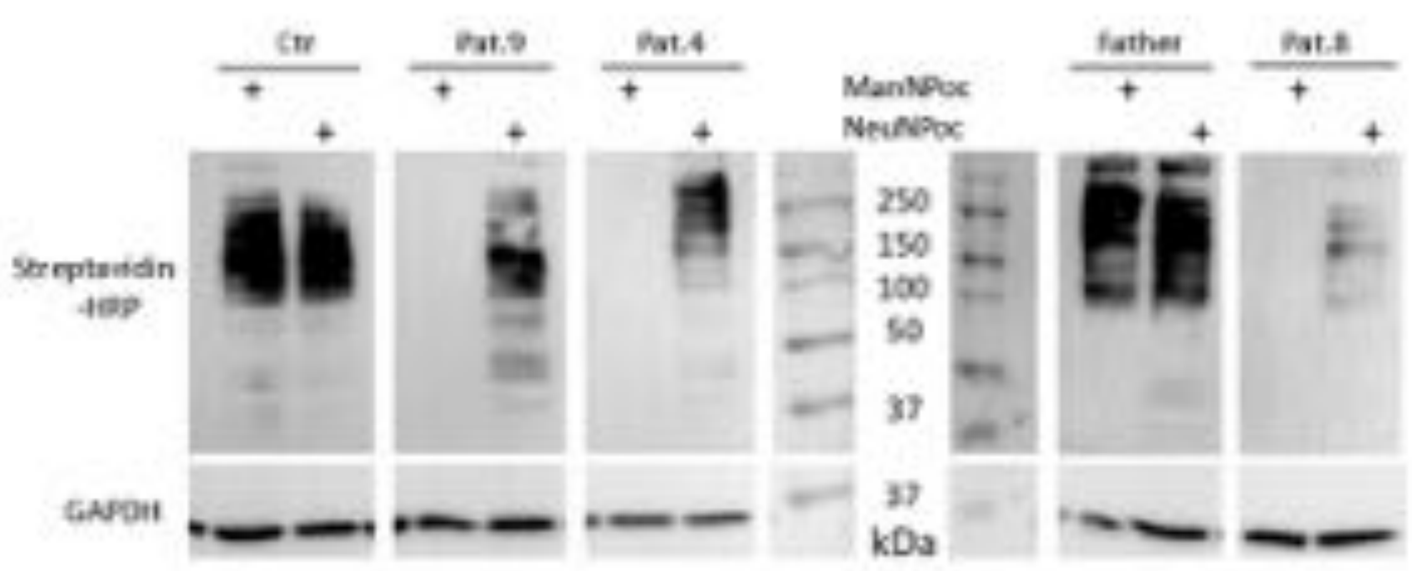
Ctr
Pat.9
Pat.4
Father
Pat.8
ManNPoc
NeuNPoc
Streptavidin
-HRP
GAPDH
250
150
100
50
37
37
kDa

biosynthesis

uridine diphosphate-GlcNAc
(UDP-GlcNAc)

UDP

UDP-GLcNAc 2-epimerase (GNE) / ManNAc 6-kinase*

N-acetyl-D-mannosamine
(ManNAc)

ATP

ADP

ManNPoc

ManNAc 6-P

N-acetyl neuraminic acid synthase (NANS)

PEP

Pi

NeuNAc 9-P

NeuNAc 9-phosphate phosphatase (NANP)

Pi

NeuNAc

CMP-sialic acid synthase (CMAS)**

CTP

PPi

NeuNPoc

CMP-NeuNAc

SLC35A1

medial and trans-Golgi

sialylation

CMP-NeuNAc

CMP

glycoproteins
glycolipids

sialoglycoproteins
sialoglycolipids

sialyltransferases

salvage

free
NeuNAc

pinocytosis

lysosome

NeuNAc

SLC17A5

NeuNAc

sialoglycoproteins
sialoglycolipids

glycoproteins
glycolipids

sialidases

de-sialylation

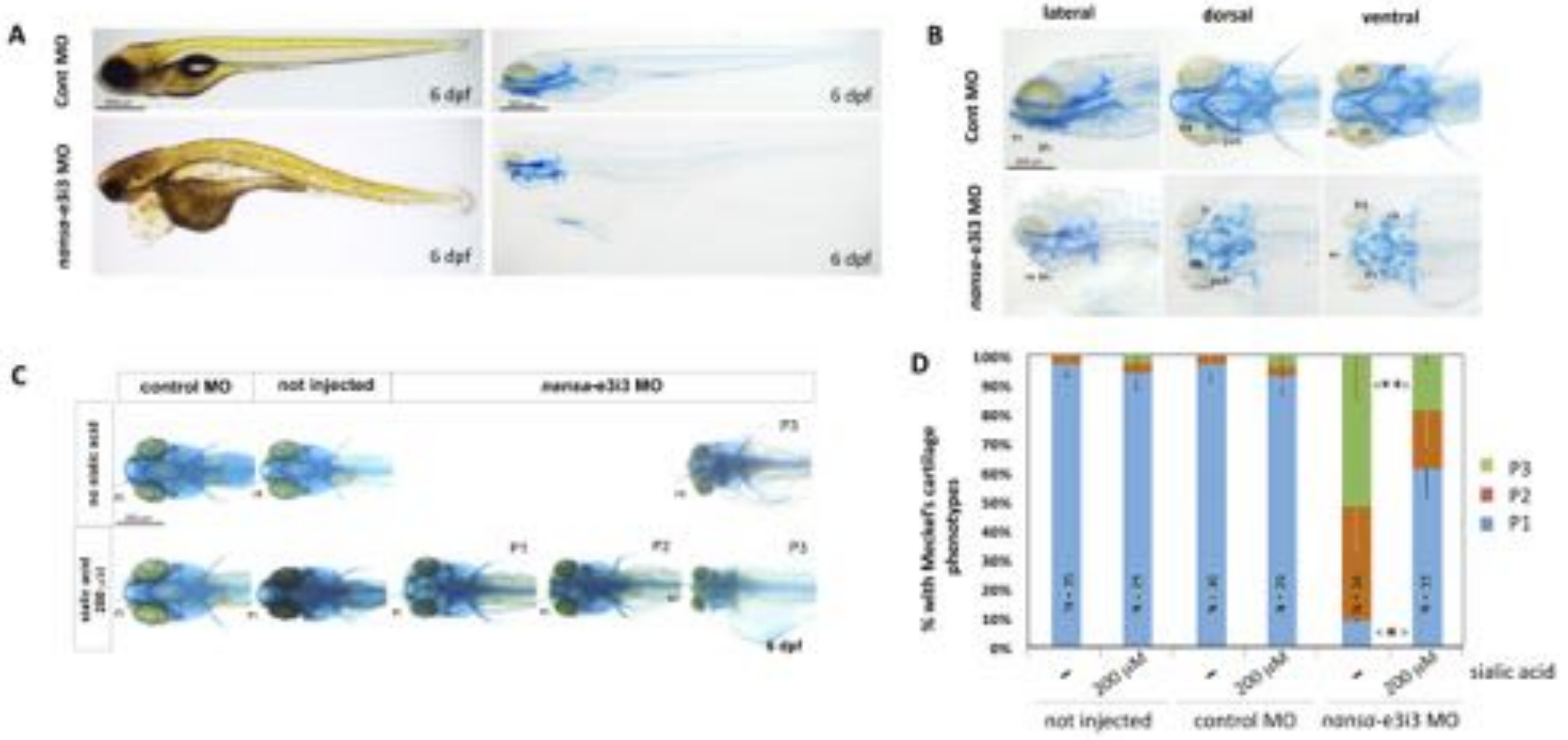
A
Cont MO
nansa-e3i3 MO
6 dpf
6 dpf
6 dpf
6 dpf
B
lateral
dorsal
ventral
Cont MO
nansa-e3i3 MO
C
control MO
not injected
nansa-e3i3 MO
no sialic acid
sialic acid 200 mM
P1
P2
P3
6 dpf
D
% with Meckel's cartilage phenotypes
100%
90%
80%
70%
60%
50%
40%
30%
20%
10%
0%
P3
P2
P1
sialic acid
not injected
control MO
nansa-e3i3 MO